J|A|C|S
ARTICLES
Published on Web 11/10/2004

Photovoltaic Cells Using Composite Nanoclusters of Porphyrins and Fullerenes with Gold Nanoparticles

Taku Hasobe,[†,‡] Hiroshi Imahori,*[,§] Prashant V. Kamat,*[,‡] Tae Kyu Ahn,[||,⊥] Seong Keun Kim,[⊥] Dongho Kim,*[,||] Atsushi Fujimoto,[§] Tsutomu Hirakawa,[‡] and Shunichi Fukuzumi*[,†]

Contribution from the Department of Material and Life Science, Graduate School of Engineering, Osaka University, CREST, Japan Science and Technology Agency (JST), Suita, Osaka 565-0871, Japan, Notre Dame Radiation Laboratory, University of Notre Dame, Notre Dame, Indiana 46556-0579, Department of Molecular Engineering, Graduate School of Engineering, Kyoto University, PRESTO, Japan Science and Technology Agency (JST), Katsura, Nishikyo-ku, Kyoto 615-8510, Japan, Fukui Institute for Fundamental Chemistry, Kyoto University, 34-4, Takano-Nishihiraki-cho, Sakyo-ku, Kyoto 606-8103, Japan, Center for Ultrafast Optical Characteristics Control, Department of Chemistry, Yonsei University, Seoul 120-749, Korea, and School of Chemistry, Seoul National University, Seoul 151-747, Korea

Received April 18, 2004; E-mail: fukuzumi@chem.eng.osaka-u.ac.jp; imahori@scl.kyoto-u.ac.jp; kamat@hertz.rad.nd.edu; dongho@yonsei.ac.kr

Abstract: Novel organic solar cells have been prepared using quaternary self-organization of porphyrin (donor) and fullerene (acceptor) units by clusterization with gold nanoparticles on nanostructured SnO_2 electrodes. First, porphyrin-alkanethiolate monolayer-protected gold nanoparticles (H_2PC*n*MPC: *n* is the number of methylene groups in the spacer) are prepared (secondary organization) starting from the primary component (porphyrin-alkanethiol). These porphyrin-modified gold nanoparticles form complexes with fullerene molecules (tertiary organization), and they are clusterized in acetonitrile/toluene mixed solvent (quaternary organization). The highly colored composite clusters can then be assembled as three-dimensional arrays onto nanostructured SnO_2 films to afford the OTE/SnO_2/(H_2PC*n*MPC+C_{60})$_m$ electrode using an electrophoretic deposition method. The film of the composite clusters with gold nanoparticle exhibits an incident photon-to-photocurrent efficiency (IPCE) as high as 54% and broad photocurrent action spectra (up to 1000 nm). The power conversion efficiency of the OTE/SnO_2/(H_2PC15MPC+C_{60})$_m$ composite electrode reaches as high as 1.5%, which is 45 times higher than that of the reference system consisting of the both single components of porphyrin and fullerene.

Introduction

The requirement to develop inexpensive and renewable energy resources has stimulated new approaches for the production of efficient, low-cost organic solar cells.[1−7] One of the most attractive strategies is the development of organic solar cells that mimic natural photosynthesis in the conversion and storage of solar energy. The three-dimensional X-ray crystal structures of reaction centers of *Rhodobacter* (Rb.) *sphaeroides*[8] and other purple bacteria including *Rhodopseudomonas* (Rh.) *viridis*[9] have provided valuable insight into such development of organic solar cells mimicking photosynthesis. A large number of pigment molecules, collectively referred to as antenna, harvest light covering a wide spectral range of the solar irradiation and transfer the light energy to the reaction center, where the actual energy

[†] Osaka University.
[‡] University of Notre Dame.
[§] Kyoto University.
[||] Yonsei University.
[⊥] Seoul National University.

(1) (a) Hagfeldt, A.; Grätzel, M. *Acc. Chem. Res.* **2000**, *33*, 269−277. (b) Grätzel, M. *Nature* **2001**, *414*, 338−344. (c) Bignozzi, C. A.; Argazzi, R.; Kleverlaan, C. J. *Chem. Soc. Rev.* **2000**, *29*, 87−96.
(2) (a) Yu, G.; Gao, J.; Hummelen, J. C.; Wudl, F.; Heeger, A. J. *Science* **1995**, *270*, 1789−1791. (b) Wudl, F. *J. Mater. Chem.* **2002**, *12*, 1959−1963.
(3) (a) Shaheen, S. E.; Brabec, C. J.; Sariciftci, N. S.; Padinger, F.; Fromherz, T.; Hummelen, J. C. *Appl. Phys. Lett.* **2001**, *78*, 841−843. (b) Padinger, F.; Rittberger, R. S.; Sariciftci, N. S. *Adv. Funct. Mater.* **2003**, *13*, 85−88.
(4) (a) Schmidt-Mende, L.; Fechtenkötter, A.; Müllen, K.; Moons, E.; Friend, R. H.; MacKenzie, J. D. *Science* **2001**, *293*, 1119−1122. (b) Halls, J. J. M.; Walsh, C. A.; Greenham, N. C.; Marseglia, E. A.; Friend, R. H.; Moratti, S. C.; Holmes, A. B. *Nature* **1995**, *376*, 498−500.
(5) (a) Granström, M.; Petritsch, K.; Arias, A. C.; Lux, A.; Andersson, M. R.; Friend, R. H. *Nature* **1998**, *395*, 257−260. (b) Huynh, W. U.; Dittmer, J. J.; Alivisatos, A. P. *Science* **2002**, *295*, 2425−2427. (c) Scher, E. C.; Manna, L.; Alivisatos, A. P. *Philos. Trans. R. Soc. London, Ser. A* **2003**, *361*, 241−255. (d) Liu, J.; Tanaka, T.; Sivula, K.; Alivisatos, A. P.; Fréchet, J. M. J. *J. Am. Chem. Soc.* **2004**, *126*, 6550−6551.
(6) (a) Wienk, M. M.; Kroon, J. M.; Verhees, W. J. H.; Knol, J.; Hummelen, J. C.; van Hal, P. A.; Janssen, R. A. J. *Angew. Chem., Int. Ed.* **2003**, *42*, 3371−3375. (b) Dhanabalan, A.; van Duren, J. K. J.; van Hal, P. A.; van Dongen, J. L. J.; Janssen, R. A. J. *Adv. Funct. Mater.* **2001**, *11*, 255−262. (c) Peumans, P.; Uchida, S.; Forrest, S. R. *Nature* **2003**, *425*, 158−162.
(7) (a) Eckert, J.-F.; Nicoud, J.-F.; Nierengarten, J.-F.; Liu, S.-G.; Echegoyen, L.; Barigelletti, F.; Armaroli, N.; Ouali, L.; Krasnikov, V.; Hadziioannou, G. *J. Am. Chem. Soc.* **2000**, *122*, 7467−7479. (b) Lahav, M.; Heleg-Shabtai, V.; Wasserman, J.; Katz, E.; Willner, I.; Dürr, H.; Hu, Y.-Z.; Bossmann, S. H. *J. Am. Chem. Soc.* **2000**, *122*, 11480−11487.
(8) Ermler, U.; Fritzsch, G.; Buchanan, S. K.; Michel, H. *Structure* **1994**, *2*, 925−936.
(9) (a) Deisenhofer, J.; Michel, H. *Science* **1989**, *245*, 1463−1473. (b) Hoff, A. J.; Deisenhofer, J. *Phys. Rep.* **1997**, *287*, 2−247.

 10.1021/ja047768u CCC: $30.25

conversion event takes place.[10] Although the strategies to design artificial photoconversion devices do not necessarily imitate all of the intricacies of natural photosynthesis, the artificial photoconversion devices developed so far have a limited degree of self-organization, whereas the components in the natural system are highly organized in quaternary protein structures.

We have established recently porphyrin-alkanethiolate monolayer protected-gold nanoclusters with spherical shape.[11] They exhibit high light-harvesting capability and suppress undesirable energy transfer quenching of the porphyrin singlet excited state by the gold surface relative to the bulk gold.[11] It should be emphasized that preorganized porphyrin molecules on gold nanoparticle possess a suitable void space[11,12] between the porphyrin moieties, which can interact with acceptor molecules. Porphyrin and fullerene have been found to be an ideal donor (D)−acceptor (A) couple, because the combination of porphyrin and fullerene results in a small reorganization energy, which allows one to accelerate photoinduced electron transfer and to slow charge recombination, leading to the generation of a long-lived charge-separated state with a high quantum yield.[13−16] Taking into account the fact that porphyrin and fullerene tend to make a supramolecular complex in solutions as well as in the solid state,[12,17−22] fullerene is expected to interact with H_2-PC*n*MPC, which would yield D−A nanoclusters with an interpenetrating network. Thus, a combination of H_2PC*n*MPC and C_{60} provides an ideal system for fulfilling an enhanced light-harvesting efficiency of chromophores throughout the solar spectrum and a highly efficient conversion of the harvested light into the high energy state of the charge separation by photoinduced electron transfer.

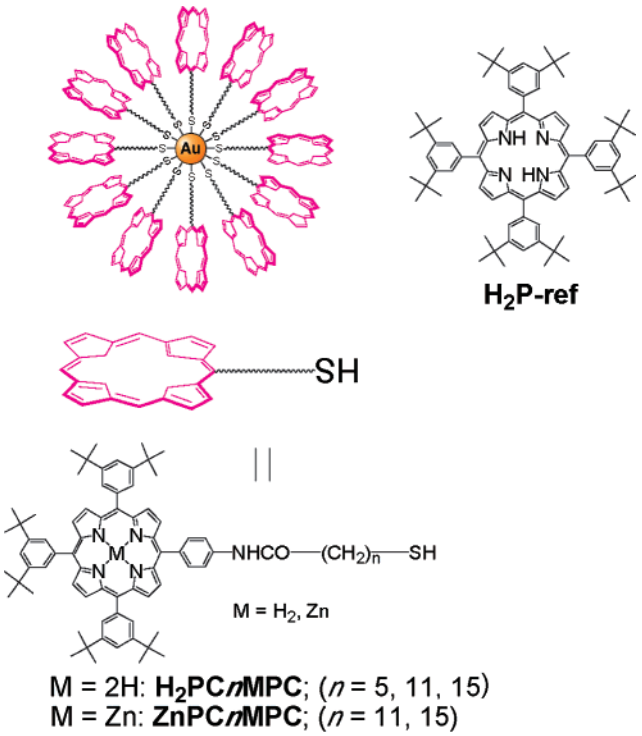

Figure 1. Porphyrin compounds used in this study.

We have recently reported novel organic solar cells composed of porphyrin gold nanoparticles (Figure 1) and fullerenes which are prepared using quaternary self-organization of porphyrin (donor) and fullerene (acceptor) moieties by clusterization with gold nanoparticles on SnO_2 electrodes as a preliminary communication.[23] Herein, we report a full report including the effects of the chain length of the spacer in H_2PC*n*MPC (n = 5, 11, and 15) and ZnPC*n*MPC (n = 11 and 15) and of the types of porphyrins (H_2P vs ZnP) and fullerenes (C_{60} vs C_{70}) on the structures and photoelectrochemical properties of the H_2-PC*n*MPC−C_{60} composite electrodes. The power conversion efficiency is now improved up to 1.5%, which is 2.5 times better than the value reported in a preliminary communication.[23] The time-resolved fluorescence decay profiles of the electrodes, femtosecond transient absorption spectra, and electron spin resonance (ESR) of the composite molecular clusters are also

(10) Williams, J. C.; Taguchi, A. K. W. Genetic manipulations of purple photosynthetic bacteria. In *Anoxygenic Photosynthetic Bacteria*; Blankenship, R. E., Madigan, M. T., Bauer, C. E., Eds.; Kluwer Academic Publishers: Dordrecht, The Netherlands, 1995; Vol. 2, pp 1029−1065.
(11) (a) Imahori, H.; Arimura, M.; Hanada, T.; Nishimura, Y.; Yamazaki, I.; Sakata, Y.; Fukuzumi, S. *J. Am. Chem. Soc.* **2001**, *123*, 335−336. (b) Imahori, H.; Kashiwagi, Y.; Endo, Y.; Hanada, T.; Nishimura, Y.; Yamazaki, I.; Araki, Y.; Ito, O.; Fukuzumi, S. *Langmuir* **2004**, *20*, 73−81. (c) Imahori, H.; Kashiwagi, Y.; Hanada, T.; Endo, Y.; Nishimura, Y.; Yamazaki, I.; Fukuzumi, S. *J. Mater. Chem.* **2003**, *13*, 2890−2898. (d) Fukuzumi, S.; Endo, Y.; Kashiwagi, Y.; Araki, Y.; Ito, O.; Imahori, H. *J. Phys. Chem. B* **2003**, *107*, 11979−11986.
(12) (a) Evans, D. R.; Fackler, N. L. P.; Xie, Z.; Rickard, C. E. F.; Boyd, P. D. W.; Reed, C. A. *J. Am. Chem. Soc.* **1999**, *121*, 8466−8474. (b) Sun, D.; Tham, F. S.; Reed, C. A.; Chaker, L.; Burgess, M.; Boyd, P. D. W. *J. Am. Chem. Soc.* **2000**, *122*, 10704−10705. (c) Nishioka, T.; Tashiro, K.; Aida, T.; Zheng, J.-Y.; Kinbara, K.; Saigo, K.; Sakamoto, S. Yamguchi, K. *Macromolecules* **2000**, *33*, 9182−9184. (d) Tashiro, K.; Aida, T.; Zheng, J.-Y.; Kinbara, K.; Saigo, K.; Sakamoto, S.; Yamaguchi, K. *J. Am. Chem. Soc.* **1999**, *121*, 9477−9478. (e) Shoji, Y.; Tashiro, K.; Aida, T. *J. Am. Chem. Soc.* **2004**, *126*, 6570−6571.
(13) Gust, D.; Moore, T. A.; Moore, A. L. *Acc. Chem. Res.* **2001**, *34*, 40−48.
(14) (a) Choi, M.-S.; Aida, T.; Luo, H.; Araki, Y.; Ito, O. *Angew. Chem., Int. Ed.* **2003**, *42*, 4060−4063. (b) Li, K.; Schuster, D. I.; Guldi, D. M.; Herranz, M. A.; Echegoyen, L. *J. Am. Chem. Soc.* **2004**, *126*, 3388−3389. (c) D'Souza, F.; Deviprasad, G. R.; El-Khouly, M. E.; Fujitsuka, M.; Ito, O. *J. Am. Chem. Soc.* **2001**, *123*, 5277−5284. (d) Armaroli, N.; Marconi, G.; Echegoyen, L.; Bourgeois, J.-P.; Diederich, F. *Chem.-Eur. J.* **2000**, *6*, 1629−1645. (e) D'Souza, F.; Smith, P. M.; Zandler, M. E.; McCarty, A. L.; Itou, M.; Araki, Y.; Ito, O. *J. Am. Chem. Soc.* **2004**, *126*, 7898−7907.
(15) (a) Fukuzumi, S.; Imahori, H. In *Electron Transfer in Chemistry*; Balzani, V., Ed.; Wiley-VCH: Weinheim, 2001; Vol. 2, pp 927−975. (b) Imahori, H.; Sakata, Y. *Eur. J. Org. Chem.* **1999**, 2445−2457. (c) Fukuzumi, S.; Guldi, D. M. In *Electron Transfer in Chemistry*; Balzani, V., Ed.; Wiley-VCH: Weinheim, 2001; Vol. 2, pp 270−337. (d) Imahori, H. *Org. Biomol. Chem.* **2004**, *2*, 1425−1433. (e) Imahori, H. *J. Phys. Chem. B* **2004**, *108*, 6130−6143. (f) Imahori, H.; Fukuzumi, S. *Adv. Funct. Mater.* **2004**, *14*, 525−536.
(16) (a) Imahori, H.; Tamaki, K.; Guldi, D. M.; Luo, C.; Fujitsuka, M.; Ito, O.; Sakata, Y.; Fukuzumi, S. *J. Am. Chem. Soc.* **2001**, *123*, 2607−2617. (b) Imahori, H.; Guldi, D. M.; Tamaki, K.; Yoshida, Y.; Luo, C.; Sakata, Y.; Fukuzumi, S. *J. Am. Chem. Soc.* **2001**, *123*, 6617−6628.
(17) Diederich, F.; Gómez-López, M. *Chem. Soc. Rev.* **1999**, *28*, 263−277.
(18) (a) Boyd, P. D. W.; Hodgson, M. C.; Rickard, C. E. F.; Oliver, A. G.; Chaker, L.; Brothers, P. J.; Bolskar, R. D.; Tham, F. S.; Reed, C. A. *J. Am. Chem. Soc.* **1999**, *121*, 10487−10495. (b) Sun, D.; Tham, F. S.; Reed, C. A.; Chaker, L.; Boyd, P. D. W. *J. Am. Chem. Soc.* **2002**, *124*, 6604−6612.
(19) Sun, D.; Tham, F. S.; Reed, C. A.; Boyd, P. D. W. *Proc. Natl. Acad. Sci. U.S.A.* **2002**, *99*, 5088−5092.
(20) (a) Olmstead, M. M.; Costa, D. A.; Maitra, K.; Noll, B. C.; Phillips, S. L.; Van Calcar, P. M.; Balch, A. L. *J. Am. Chem. Soc.* **1999**, *121*, 7090−7097. (b) Olmstead, M. M.; de Bettencourt-Dias, A.; Duchamp, J. C.; Stevenson, S.; Marciu, D.; Dorn, H. C.; Balch, A. L. *Angew. Chem., Int. Ed.* **2001**, *40*, 1223−1225.
(21) (a) Zheng, J.-Y.; Tashiro, K.; Hirabayashi, Y.; Kinbara, K.; Saigo, K.; Aida, T.; Sakamoto, S.; Yamaguchi, K. *Angew. Chem., Int. Ed.* **2001**, *40*, 1857−1861. (b) Shirakawa, M.; Fujita, N.; Shinkai, S. *J. Am. Chem. Soc.* **2003**, *125*, 9902−9903.
(22) (a) Guldi, D. M.; Luo, C.; Prato, M.; Troisi, A.; Zerbetto, F.; Scheloske, M.; Dietel, E.; Bauer, W.; Hirsch, A. *J. Am. Chem. Soc.* **2001**, *123*, 9166−9167. (b) Imahori, H.; Hagiwara, K.; Aoki, M.; Akiyama, T.; Taniguchi, S.; Okada, T.; Shirakawa, M.; Sakata, Y. *J. Am. Chem. Soc.* **1996**, *118*, 11771−11782. (c) Wang, Y.-B.; Lin, Z. *J. Am. Chem. Soc.* **2003**, *125*, 6072−6073. (d) Imahori, H.; Tkachenko, N. V.; Vehmanen, V.; Tamaki, K.; Lemmetyinen, H.; Sakata, Y.; Fukuzumi, S. *J. Phys. Chem. A* **2001**, *105*, 1750−1756. (e) Tkachenko, N. V.; Guenther, C.; Imahori, H.; Tamaki, K.; Sakata, Y.; Fukuzumi, S.; Lemmetyinen, H. *Chem. Phys. Lett.* **2000**, *326*, 344−350.
(23) A preliminary report has appeared: Hasobe, T.; Imahori, H.; Kamat, P. V.; Fukuzumi, S. *J. Am. Chem. Soc.* **2003**, *125*, 14962−14963.

Scheme 1

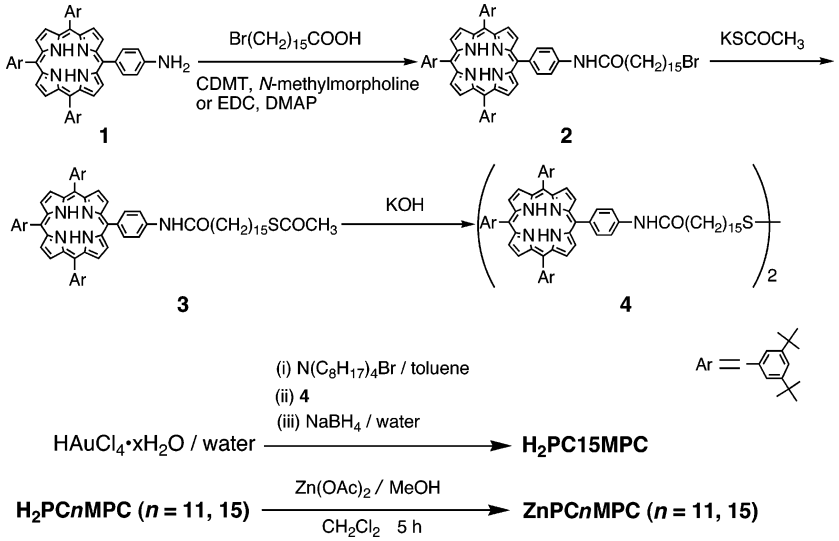

reported, providing valuable mechanistic insight into the photocurrent generation.

Experimental Section

General. Melting points were recorded on a Yanagimoto micro-melting point apparatus and were not corrected. ^{1}H NMR spectra were measured on a JEOL EX-270 (270 MHz) or a JEOL JMN-AL300 (300 MHz) spectrometer. Matrix-assisted laser desorption/ionization (MALDI) time-of-flight mass spectra (TOF) were measured on a Kratos Compact MALDI I (Shimadzu) spectrometer.

Materials. All solvents and chemicals were of reagent grade quality, obtained commercially, and used without further purification unless otherwise noted (vide infra). Thin-layer chromatography (TLC) and flash column chromatography were performed with Art. 5554 DC-Alufolien Kieselgel 60 F_{254} (Merck) and Fujisilicia BW300, respectively. Nanostructured SnO_2 films were cast on an optically transparent electrode (OTE) by applying a 2% colloidal solution obtained from Alfa Chemicals. The air-dried films were annealed at 673 K. The details of the preparation of SnO_2 films on conducting glass substrate were reported elsewhere.[24] The nanostructured SnO_2 film electrode is referred to as OTE/SnO_2.

Electrophoretic Deposition of Cluster Films. A known amount of porphyrin derivatives, C_{60} or a mixed cluster solution in acetonitrile/toluene (3/1, v/v, 2 mL), was transferred to a 1 cm cuvette in which two electrodes (viz., OTE/SnO_2 and OTE) were kept at a distance of 6 mm using a Teflon spacer. A DC voltage (200 V) was applied between these two electrodes using a Fluke 415 power supply. The deposition of the film can be visibly seen as the solution becomes colorless with simultaneous brown coloration of the OTE/SnO_2 electrode. The OTE/SnO_2 electrode coated with mixed H_2PC*n*MPC and C_{60} clusters is referred to OTE/SnO_2/(H_2PC*n*MPC+C_{60})$_m$.

The UV−visible spectra were recorded on a Shimadzu 3101 spectrophotometer. Transmission electron micrographs (TEM) of composite clusters were recorded by applying a drop of the sample to a carbon-coated copper grid. Images were recorded using a Hitachi H600 transmission electron microscope. AFM measurements were carried out using a Digital Nanoscope III in the tapping mode. Dynamic light scattering studies were carried out using a Horiba LB-550 instrument.

Photoelectrochemical Measurements. Photoelectrochemical measurements were carried out in a standard two-compartment cell consisting of a working electrode and a Pt wire gauze counter. All other photoelectrochemical measurements were carried out using a working electrode and a Pt gauge counter electrode in the same cell assembly using a Keithley model 617 programmable electrometer. The electrolyte was 0.5 M NaI and 0.01 M I_2 in acetonitrile. A collimated light beam from a 150 W xenon lamp with a 400 nm cutoff filter was used for excitation of (H_2PC*n*MPC+C_{60})$_m$ films deposited on SnO_2 electrodes. A Bausch and Lomb high-intensity grating monochromator was introduced into the path of the excitation beam for the selected wavelength.

Photodynamics Measurements. Quenching experiments of the fluorescence of (H_2PC*n*MPC+C_{60})$_m$ or (ZnPC15MPC+C_{60})$_m$ were carried out on a SHIMADZU spectrofluorophotometer (RF-5000). Fluorescence decays were measured by using femtosecond pulse laser excitation and a single photon counting system for fluorescence decay measurements.[25] The laser system was a cavity-dumped femtosecond Ti:Sa laser pumped by a cw Nd:YAG laser (Spectra-Physics, Millenia). The full width at half-maximum of the instrument response function was 53 ps. The fluorescence decays were measured with magic angle emission polarization. Femtosecond laser flash photolysis experiments were conducted using a Clark-MXR 2010 laser system (387 nm excitation pulse of fwhm 150 fs) and an Ultrafast detection system. The details of the femtosecond laser flash photolysis experiments are given in the Supporting Information (S1).

ESR Measurements. A quartz ESR tube (internal diameter: 4.5 mm) containing a deaerated acetonitrile/toluene (3/1, v/v) solution of (H_2PC15MPC+C_{60})$_m$ was irradiated in the cavity of the ESR spectrometer with the focused light of a 1000-W high-pressure Hg lamp (Ushio-USH1005D) through an aqueous filter at low temperature. The ESR spectra in frozen acetonitrile/toluene were measured under nonsaturating microwave power conditions using a JEOL X-band spectrometer (JES-RE1XE) with an attached variable temperature apparatus. The magnitude of modulation was chosen to optimize the resolution and the signal-to-noise (S/N) ratio of the observed spectra when the maximum slope line width (H_{msl}) of the ESR signals was unchanged with a larger modulation magnitude. The *g* values were calibrated with an Mn^{2+} marker.

Results and Discussion

Synthesis. The synthetic strategy in this work is shown in Scheme 1. The preparation of free base porphyrin−gold cluster (H_2PC*n*MPC: *n* = 11 and 5) and starting material of 5-(4-aminophenyl)-10,15,20-tris(3,5-di-*tert*-butylphenyl)porphyrin **1**

(24) Bedja, I.; Hotchandani, S.; Kamat, P. V. *J. Phys. Chem.* **1994**, *98*, 4133−4140.

(25) Yamada, H.; Imahori, H.; Nishimura, Y.; Yamazaki, I.; Ahn, T. K.; Kim, S. K.; Kim, D.; Fukuzumi, S. *J. Am. Chem. Soc.* **2003**, *125*, 9129−9139.

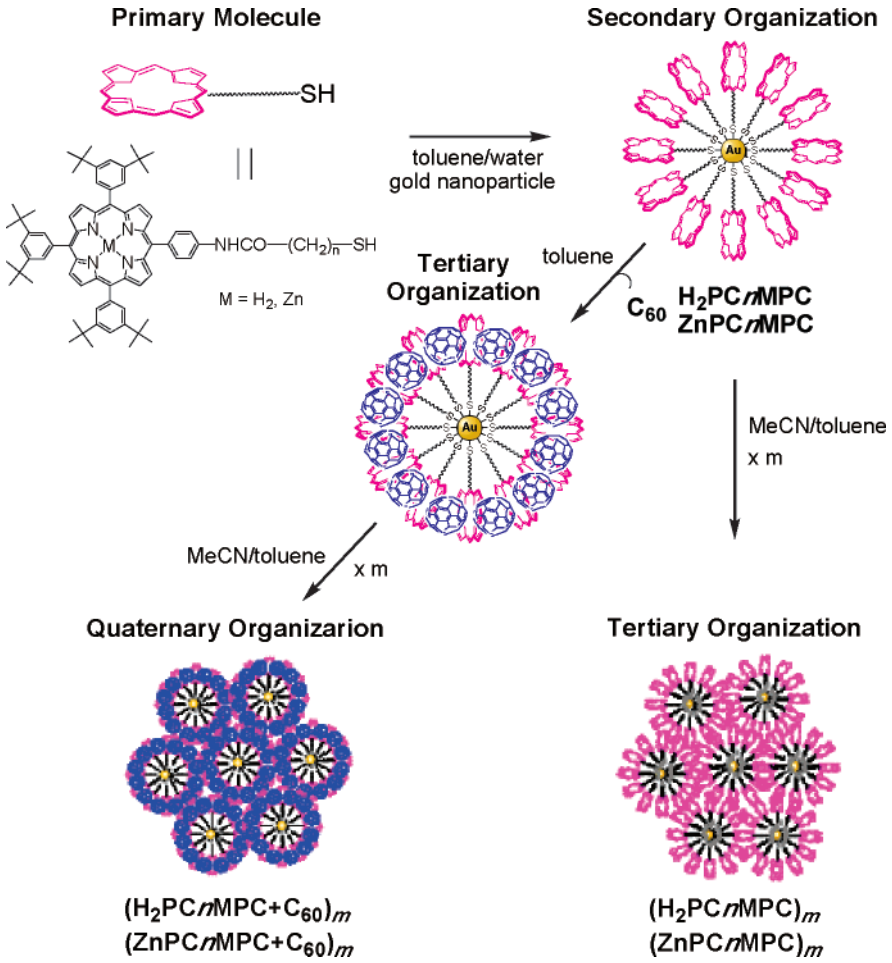

Figure 2. Illustration of high order organization.

has been described elsewhere.[11,22b,26] Condensation of this aminoporphyrin **1** with 16-bromohexanoic acid in the presence of 1-[3-(dimethylamino)propyl]-3-ethylcarbodiimide (EDC) and 4-(dimethylamino)pyridine (DMAP) afforded **2**. Bromide **2** was converted to porphyrin disulfide **4** via thioesterification with potassium thioacetate and subsequent base deprotection of **3**. H_2PC15MPC was directly prepared by reduction of $HAuCl_4$ with $NaBH_4$ in toluene/water containing porphyrin disulfide (**4**: $HAuCl_4$ = 1:2) to increase the extent of functionalization. A detailed procedure of the synthesis is described in the Supporting Information (S2, S3).

Assembly of Free Base Porphyrin and C_{60} as Molecular Clusters in Mixed Solvents. H_2PC*n*MPC and C_{60} are soluble in nonpolar solvents such as toluene, but sparingly soluble in polar solvents such as acetonitrile. When a concentrated solution of H_2PC*n*MPC or C_{60} in toluene is mixed with acetonitrile by a fast injection method, the molecules aggregate to form stable clusters.[27] The final solvent ratio of mixed solvent employed in the present experiments was 3:1 (v/v) acetonitrile:toluene. The same strategy can be extended to prepare mixed or composite molecular clusters consisting of H_2PC*n*MPC and C_{60} molecules. Mixed cluster aggregates in the present investigation were prepared by mixing equimolar solution of H_2PC*n*MPC and C_{60} in toluene (0.5 mL) and then injecting them into a pool of acetonitrile (1.5 mL). These optically transparent composite clusters are stable at room temperature, and they can be reverted back to their monomeric forms by diluting the solution with toluene.[27]

Figure 2 summarizes the procedure of high-order self-organization of porphyrin (donor) and fullerene (acceptor) moieties by clusterization. First, porphyrin-alkanethiolate monolayer protected-gold nanoclusters with spherical shape (H_2-PC*n*MPC)[11] are prepared (secondary organization) starting from porphyrin-alkanethiol (primary molecule). Taking the gold core as a sphere with density ρ_{Au} (58.01 atoms/nm^3) covered with an outermost layer of hexagonally close-packed gold atoms (13.89 atoms/nm^2) with a radius of $R_{CORE} - R_{Au}$ (R_{Au} = 0.145 nm), the model predicts that the core of H_2PC11MPC contains 280 Au atoms, of which 143 lie on the Au surface. Given the values of the elemental analysis of H_2PC11MPC (H, 4.88%; C, 44.77%; N, 3.10%), there are 57 porphyrin-alkanethiolate chains on the gold surface for H_2PC11MPC. These nanoparticles form complexes with fullerene molecules (tertiary organization),

(26) (a) Takagi, S.; Miyamoto, T. K.; Sasaki, Y. *Bull. Chem. Soc. Jpn.* **1986**, *59*, 2371−2373. (b) Tkachenko, N. V.; Lemmetyinen, H.; Sonoda, J.; Ohkubo, K.; Sato, T.; Imahori, H.; Fukuzumi, S. *J. Phys. Chem. A* **2003**, *107*, 8834−8844. (c) Imahori, H.; Norieda, H.; Nishimura, Y.; Yamazaki, Y.; Higuchi, K.; Kato, N.; Motohiro, T.; Yamada, H.; Tamaki, K.; Arimura, M.; Sakata, Y. *J. Phys. Chem. B* **2000**, *104*, 1253−1260.

(27) (a) Kamat, P. V.; Barazzouk, S.; Thomas, K. G.; Hotchandani, S. *J. Phys. Chem. B* **2000**, *104*, 4014−4017. (b) Sudeep P. K.; Ipe, B. I.; Thomas, K. G.; George, M. V.; Barazzouk, S.; Hotchandani, S.; Kamat, P. V. *Nano Lett.* **2002**, *2*, 29−35. (c) Kamat, P. V.; Barazzouk, S.; Hotchandani, S.; Thomas, K. G. *Chem.-Eur. J.* **2000**, *6*, 3914−3921.

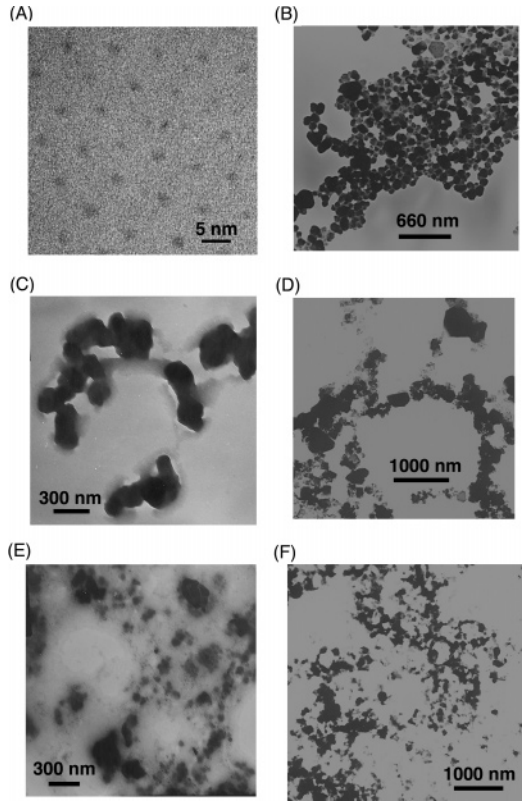

Figure 3. TEM images of (A) H_2PC15MPC (1.0 mM) in toluene, (B) $(H_2$-PC15MPC+$C_{60})_m$ ([H_2P] = 0.19 mM; [C_{60}] = 0.31 mM) in acetonitrile/toluene = 3/1 (v/v), (C) (H_2PC11MC+$C_{60})_m$ ([H_2P] = 0.19 mM; [C_{60}] = 0.31 mM) in acetonitrile/toluene = 3/1 (v/v), (D) (H_2PC5MPC+$C_{60})_m$ ([H_2P] = 0.19 mM; [C_{60}] = 0.31 mM) in acetonitrile/toluene = 3/1 (v/v), (E) (H_2PC11MC)$_m$ ([H_2P] = 0.19 mM) in acetonitrile/toluene = 3/1 (v/v), and (F) (H_2P-ref+$C_{60})_m$ ([H_2P] = 0.19 mM; [C_{60}] = 0.31 mM) in acetonitrile/toluene = 3/1 (v/v).

and they are clusterized in acetonitrile/toluene mixed solvent (quaternary organization).

The clusters of (H_2PC11MPC+$C_{60})_m$, (H_2PC11MPC)$_m$, and ($C_{60})_m$ were characterized using the dynamic light scattering method. In toluene, the average diameter of H_2PC11MPC was determined as 7 ± 2 nm, which is consistent with the value (9 nm) estimated by molecular modeling (vide infra). In a mixture (3:1) of acetonitrile−toluene, the size distribution of clusters of (H_2PC11MPC+$C_{60})_m$, (H_2PC11MPC)$_m$, and ($C_{60})_m$ was found to be narrow with different mean diameters of 115 nm for (H_2-PC11MPC+$C_{60})_m$, 48 nm for (H_2PC11MPC)$_m$, and 163 nm for ($C_{60})_m$, as shown in Figure S4 (see Supporting Information S4). These results suggest that C_{60} molecules are incorporated into the void space between the porphyrin moieties in the porphyrin-modified gold nanoparticle to make the highly organized aggregates in the mixed solvent.

Figure 3 shows TEM images of H_2PC15MPC, the composite clusters: (H_2PC*n*MPC+$C_{60})_m$ (n = 5, 11, and 15), (H_2-PC11MPC)$_m$, and (H_2P-ref+$C_{60})_m$. As the solvent evaporates on the copper grid, the clusters form well-defined shapes and sizes. The diameter of the gold core in H_2PC15MPC is determined as 2.1 ± 0.4 nm (Figure 3A), which is virtually the same as that of H_2PC11MPC.[11] The TEM image of (H_2-PC*n*MPC+$C_{60})_m$ (n = 15, 11, and 5) (Figure 3B−D) displays a more efficient network structure as compared to the TEM image of (H_2PC11MPC)$_m$ without fullerene (Figure 3E) and that of (H_2P-ref+$C_{60})_m$ without gold nanoparticles (Figure 3F). In

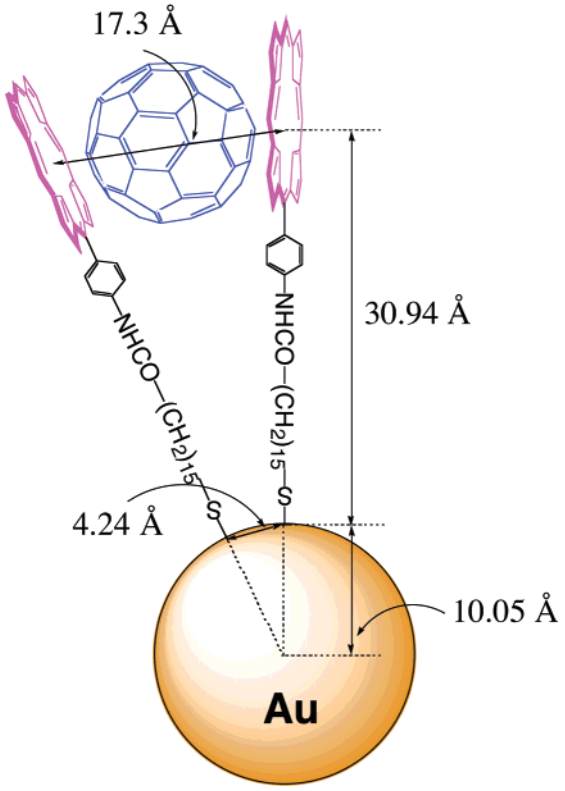

Figure 4. Insertion of C_{60} between the porphyrin rings of H_2PC15MPC.

particular, the TEM images exhibit well-controlled size and the spherical or cubic shape with diameters of 50−100 nm for (H_2-PC15MPC+$C_{60})_m$ and 200−300 nm (H_2PC11MPC+$C_{60})_m$, whereas that of (H_2PC5MPC+$C_{60})_m$ shows irregular size (50−500 nm) and random shape.[28] Such a difference in the formation of nanoclusters is largely dependent on the interaction between porphyrin and fullerene. The structures of porphyrin-alkanethiolate (n = 5, 11, and 15) on the gold nanoparticles are estimated by molecular mechanics calculations.[29] Because there are 57 porphyrin-alkanethiolate chains on the gold surface for H_2-PC11MPC (vide supra),[11] the C_{60} structure which contains 60 carbons with 7.1 Å diameter can be used for the calculation of the structure of H_2PC11MPC with a 21 Å diameter as the gold core.[11] There are two types of C−C bonds of C_{60}: 30 short "double bonds" (1.404 Å) and 60 long "single bonds" (1.448 Å).[30] The average distance between two gold atoms to which neighboring porphyrin-alkanethiolates are attached is estimated as 4.24 Å by multiplying the average length of the C−C bond (1.433 Å) by the ratio of the diameter (21 Å) of the gold core to the diameter (7.1 Å) of C_{60} as shown in Figure 4. The

(28) The molecular cluster of (ZnPC15MPC+$C_{60})_m$ has irregular size and random shape as compared to that of (H_2PC15MPC+$C_{60})_m$. This trend may be due to π-complex formation between the porphyrin and the fullerene, which is based on the difference of the apparent associate constant (vide supra). See Supporting Information S5.

(29) The distance between the center of the porphyrin ring to the gold surface is estimated as 29.9 Å (H_2PC15MPC), 24.9 Å (H_2PC11MPC), and 17.4 Å (H_2PC5MPC) on the basis of the molecular mechanics calculation of porphyrin alkanethiol. The radius of the covalent bond of sulfur (S) is taken as 1.04 Å.

(30) There are two types of C−C bonds of C_{60}: 30 short "double bonds" (1.404 Å) and 60 long "single bonds" (1.448 Å). The average length of the C−C bonds (1.433 Å) is used for the calculation of the average distance between neighboring porphyrin-alkanethiolates in H_2PC*n*MPC (n = 5, 11, and 15). See: Hirsch, A. *The Chemistry of the Fullerenes*; George Thieme Verlag: Stuttgart, New York, 1994.

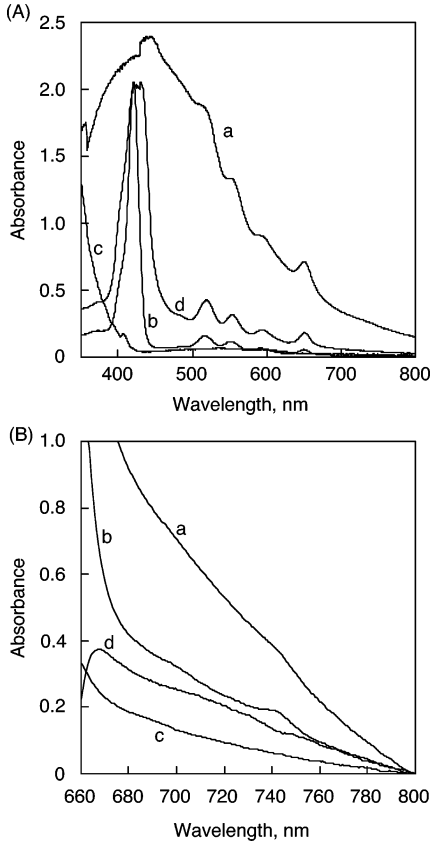

Figure 5. (A) Absorption spectra of (a) $(H_2PC11MPC+C_{60})_m$ in acetonitrile/toluene (3/1, v/v) ($[H_2P] = 0.19$ mM; $[C_{60}] = 0.31$ mM), (b) $H_2PC11MPC$ in toluene ($[H_2P] = 18$ μM), (c) C_{60} in toluene ($[C_{60}] = 150$ μM) and (d) $(H_2PC11MPC)_m$ in acetonitrile/toluene (3/1, v/v) ($[H_2P] = 0.19$ mM). (B) Absorption spectra of (a) mixed $H_2PC15MPC$ (0.8 mM) and C_{60} (5.0 mM), (b) $H_2PC15MPC$ (0.8 mM), and (c) C_{60} (5.0 mM) in *o*-dichlorobenzene. The CT absorption of $H_2PC15MPC$ (0.8 mM) and C_{60} (5.0 mM) (d) has been obtained by subtracting the absorption of (b) and (c) from (a).

schematic structure in Figure 4 affords the center-to-center distances between two porphyrins in $H_2PC5MPC$, $H_2PC11MPC$, and $H_2PC15MPC$ as 11.5, 15.2, and 17.3 Å, respectively. The closest distance between a carbon of C_{60} and the center of the porphyrin ring has been reported as 2.856 Å by the X-ray crystal structure of the C_{60} complex with a jaw-like bis-porphyrin.[12b,21a] Thus, the smallest center-to-center distance of two porphyrin rings which can accommodate C_{60} between the rings is estimated as 12.8 Å by adding the diameter of C_{60} (7.1 Å) to twice the closest distance between a carbon of C_{60} and the center of the porphyrin ring (5.7 Å). The estimated distances between two porphyrins in $H_2PC11MPC$ (15.2 Å) and $H_2PC15MPC$ (17.3 Å) are long enough for the two porphyrins to accommodate C_{60} between the rings in contrast with $H_2PC5MPC$ (11.5 Å). The longer porphyrin−porphyrin distance in $H_2PC15MPC$ than in $H_2PC11MPC$ and $H_2PC5MPC$ may result in the accommodation of more C_{60} molecules between the porphyrin rings.

The absorption spectra of $H_2PC11MPC$ and C_{60} in neat toluene are compared to that of $[(H_2PC11MPC+C_{60})_m]$ clusters in acetonitrile/toluene (3/1, v/v) in Figure 5A. The composite clusters $[(H_2PC11MPC+C_{60})_m]$ in the mixed solvent (spectrum a) exhibit much broader and more intense absorption in the visible and near-IR regions than those of parent $H_2PC11MPC$ (spectrum b) and C_{60} (spectrum c) in toluene.[31] This demonstrates that the composite clusters of $H_2PC11MPC$ and C_{60} are superior as light absorbers to the single component clusters of $H_2PC11MPC$ or C_{60}, because the composite clusters absorb throughout the visible part of the solar spectrum.

Figure 5B shows charge-transfer (CT) absorption between $H_2PC15MPC$ and C_{60}. The CT absorption is obtained by subtracting the spectrum of $H_2PC15MPC$ and C_{60} from that of composite $H_2PC15MPC$ and C_{60}. The broad absorption in the visible and near-IR regions is characteristic of the π-complex formed between porphyrins and fullerenes.[22b,d,e] A CT type interaction in the π-complex between porphyrin and fullerene molecules may be responsible for the long-wavelength absorption of the composite clusters in Figure 5A, where the spectrum of $(H_2PC\textit{n}MPC+C_{60})_m$ (spectrum a in Figure 5A) is much broader than that of $(H_2PC\textit{n}MPC)_m$ (spectrum d in Figure 5A). Similar CT interactions leading to such an extended absorption have been observed for porphyrin−C_{60} dyads linked at close proximity.[22b,d,e,32,33] Thus, we can control the three-dimensional array of porphyrins and C_{60} molecules by using gold nanoparticles.

Electrophoretic Deposition of $H_2PC\textit{n}MPC$ and C_{60} Mixed Clusters. As shown earlier,[34] clusters of porphyrin and C_{60} prepared in acetonitrile/toluene mixed solvent can be assembled electrophoretically as thin films on a conducting glass electrode surface. A similar electrodeposition approach was adopted to prepare films of $(H_2PC\textit{n}MPC+C_{60})_m$ on nanostructured SnO_2, which were cast on an optically conducting glass electrode (referred as OTE/SnO_2). Upon application of a DC electric field of 200 V between the OTE/SnO_2 and OTE electrodes which were immersed together in a mixed acetonitrile/toluene (3/1, v/v) solution containing $(H_2PC\textit{n}MPC+C_{60})_m$ clusters, the mixed clusters are deposited on the SnO_2 nanocrystallites. As the deposition continues, the discoloration of the solution is observed, accompanied by concomitant coloration of the electrode that is connected to the positive terminal of a DC power supply.

The absorption spectra of OTE/SnO_2/$(H_2PC\textit{n}MPC+C_{60})_m$ (n = 5, 11, and 15) electrodes prepared using $H_2PC\textit{n}MPC$ and C_{60} in acetonitrile/toluene (3/1, v/v) are shown in Figure S6 (see Supporting Information S6). The absorptivity of OTE/SnO_2/$(H_2PC\textit{n}MPC+C_{60})_m$ (spectra a−c) is much enhanced as compared to that of OTE/SnO_2/$(H_2PC\textit{n}MPC)_m$ (n = 11) (spectrum d). These results ensure that incident light is absorbed efficiently in the visible and near-IR regions by OTE/SnO_2/$(H_2PC\textit{n}MPC+C_{60})_m$. The absorption spectra of OTE/SnO_2/$(H_2PC\textit{n}MPC+C_{60})_m$ reflect those of $(H_2PC\textit{n}MPC+C_{60})_m$ in acetonitrile/toluene = 3/1, and this indicates the cluster solution is effectively deposited on OTE/SnO_2.

The AFM images of OTE/SnO_2/$(H_2PC15MPC+C_{60})_m$ and OTE/SnO_2/$(H_2PC5MPC+C_{60})_m$ reveal the cluster aggregation with a regular size as shown in Figure S7 (see Supporting Information S7). These results also suggest that the electro-

(31) A red shift of the Soret band of $H_2PC11MPC$ in composite clusters $[(H_2PC11MPC+C_{60})_m]$ (spectrum a) is recognized as compared to that of parent $H_2PC11MPC$ (spectrum b), whereas no significant shift is observed at the Q-band. This is consistent with the absorption properties of the CT complex between porphyrin and fullerene.[22]

(32) (a) D'Souza, F.; Gadde, S.; Zandler, M. E.; Arkady, K.; El-Khouly, M. E.; Fujitsuka, M.; Ito, O. *J. Phys. Chem. A* **2002**, *106*, 12393−12404. (b) Schuster, D. I.; Jarowski, P. D.; Kirschner, A. N.; Wilson, S. R. *J. Mater. Chem.* **2002**, *12*, 2041−2047.

(33) Tkachenko, N. V.; Rantala, L.; Tauber, A. Y.; Helaja, J.; Hynninen, P. H.; Lemmetyinen, H. *J. Am. Chem. Soc.* **1999**, *121*, 9378−9387.

(34) (a) Hasobe, T.; Imahori, H.; Fukuzumi, S.; Kamat, P. V. *J. Mater. Chem.* **2003**, *13*, 2515−2520. (b) Hasobe, T.; Imahori, H.; Fukuzumi, S.; Kamat, P. V. *J. Phys. Chem. B* **2003**, *107*, 12105−12112.

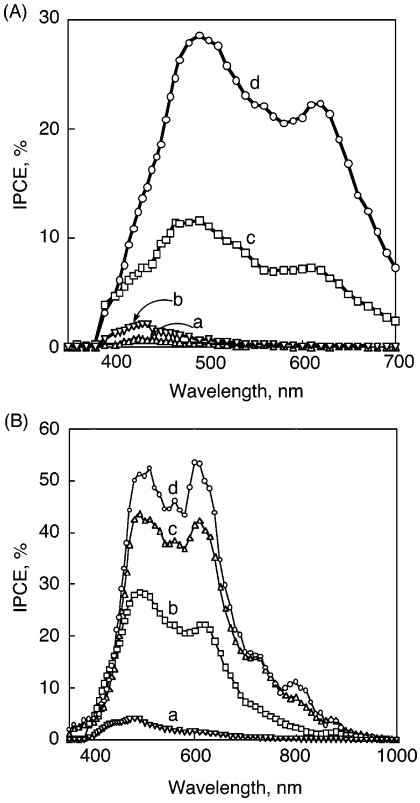

Figure 6. Photocurrent action spectra of (A) the OTE/SnO_2/(H_2PC11MPC+C_{60})$_m$ electrode ([H_2P] = 0.19 mM; [C_{60}] = (a) 0 mM, (b) 0.06 mM, (c), 0.19 mM, (d) 0.31 mM); and (B) the OTE/SnO_2/(H_2PC*n*MPC+C_{60})$_m$ electrode ([H_2P] = 0.19 mM; (a) n = 5, [C_{60}] = 0.31 mM; (b) n = 11, [C_{60}] = 0.31 mM; (c) n = 15, [C_{60}] = 0.31 mM; (d) n = 15, [C_{60}] = 0.38 mM). Electrolyte: 0.5 M NaI and 0.01 M I_2 in acetonitrile.

phoretic deposition of (H_2PC*n*MPC+C_{60})$_m$ leads to the association of clusters on the nanostructured SnO_2 electrode growing into larger ones.[23] The sizes of OTE/SnO_2/(H_2PC15MPC+C_{60})$_m$ and OTE/SnO_2/(H_2PC5MPC+C_{60})$_m$ are approximately the same (Figure S7A,B). This indicates that the step-by-step organization of porphyrin and C_{60} molecules is achieved on SnO_2, allowing the formation of the interpenetrating network of porphyrin and C_{60} molecules in OTE/SnO_2/(H_2PC*n*MPC+C_{60})$_m$.

Photoelectrochemical Properties of OTE/SnO_2/(H_2PC*n*MPC+C_{60})$_m$. To evaluate the photoelectrochemical performance of the (H_2PC*n*MPC+C_{60})$_m$ films, we used the OTE/SnO_2/(H_2PC*n*MPC+C_{60})$_m$ electrode as a photoanode in a photoelectrochemical cell. Photocurrent measurements were performed in acetonitrile containing NaI (0.5 M) and I_2 (0.01 M) as redox electrolyte using a Pt gauge counter electrode.

Photocurrent action spectra of (H_2PC*n*MPC+C_{60})$_m$ clusters are shown in Figure 6. The IPCE values were calculated by normalizing the photocurrent values for incident light energy and intensity using eq 1,[35]

$$\text{IPCE (\%)} = 100 \times 1240 \times I_{sc}/(I_{inc} \times \lambda) \qquad (1)$$

where I_{sc} is the short circuit photocurrent (A/cm^2), I_{inc} is the incident light intensity (W/cm^2), and λ is the wavelength (nm). The overall response of OTE/SnO_2/(H_2PC*n*MPC+C_{60})$_m$ parallels the broad absorption spectral features, indicating the involvement of both H_2PC*n*MPC and C_{60} in the photocurrent generation.

(35) Khazraji, A. C.; Hotchandani, S.; Das, S.; Kamat P. V. *J. Phys. Chem. B* **1999**, *103*, 4693−4700.

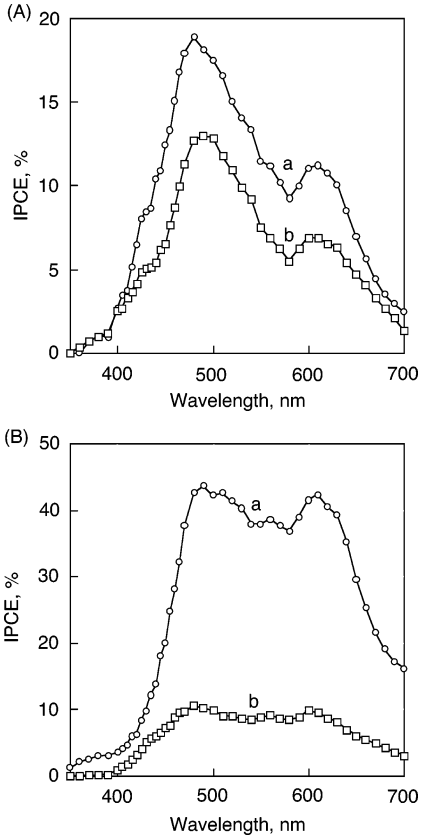

Figure 7. (A) Photocurrent action spectra of the OTE/SnO_2/(ZnPC*n*MPC+C_{60})$_m$ electrode: (a) n = 15, (b) n = 11 ([ZnP] = 0.19 mM; [C_{60}] = 0.31 mM); and (B) photocurrent action spectra of (a) the OTE/SnO_2/(H_2PC15MPC+C_{60})$_m$ electrode ([H_2P] = 0.19 mM; [C_{60}] = 0.31 mM); and (b) the OTE/SnO_2/(H_2PC15MPC+C_{70})$_m$ electrode ([H_2P] = 0.19 mM; [C_{60}] = 0.31 mM). Electrolyte: 0.5 M NaI and 0.01 M I_2 in acetonitrile.

The concentration effects of C_{60} with a constant concentration of H_2PC11MPC on the photocurrent action spectra are shown in Figure 6A, where the IPCE values of the OTE/SnO_2/(H_2PC-11MPC)$_m$ system exhibit a remarkable increase with an increase in the relative concentration of C_{60} to reach the maximum IPCE of 28% at 490 nm with the initial relative concentration of [H_2P]:[C_{60}] = 38:62. Considering the well-established photodynamics of the porphyrin−fullerene system,[15,16] the porphyrin excited singlet state may be quenched by C_{60} via electron transfer in the porphyrin−C_{60} complex rather than by gold nanocluster via energy transfer.

Figure 6B shows the effect of the alkanethiolate chain length on the IPCE values. The action spectra indicate that the higher IPCE and the broader photoresponse are attained with the longer chain length of H_2PC*n*MPC. In particular, OTE/SnO_2/(H_2PC-15MPC+C_{60})$_m$ ([H_2P] = 0.19 mM, [C_{60}] = 0.38 mM) exhibits a maximum IPCE value (54%) and a very broad photoresponse (up to ∼1000 nm) which extends to the near-IR region. In OTE/SnO_2/(H_2PC15MPC+C_{60})$_m$, a long methylene spacer of H_2-PC15MPC allows enough space for fullerene molecules to insert themselves between the neighboring two porphyrin rings effectively as compared to the clusters with a shorter methylene spacer, leading to more efficient photocurrent generation.

Free Base Porphyrin versus Zinc Porphyrin and C_{60} versus C_{70}. We have also examined the effects of the types of porphyrins (H_2P vs ZnP) and the types of fullerenes (C_{60} vs C_{70}) on the photoelectrochemical properties of the composite cluster electrodes. Figure 7A shows the photocurrent action

spectra of OTE/SnO_2/(ZnPC*n*MPC+C_{60})$_m$ (n = 11 and 15). The IPCE values of OTE/SnO_2/(ZnPC*n*MPC+C_{60})$_m$ become smaller than those of (H_2PC*n*MPC+C_{60})$_m$. In the case of zinc porphyrin, the driving force of charge separation between excited zinc porphyrin and C_{60} becomes larger as compared to free base porphyrin, because the one-electron reduction potential of the singlet excited state of ZnP (−1.0 V vs NHE) is more negative than that of H_2P,[15a] whereas the driving force of electron transfer from I^-/I_3^- to $ZnP^{\bullet+}$ is smaller than that of electron transfer to $H_2P^{\bullet+}$ due to the lower one-electron oxidation potential of ZnP (+1.0 V vs NHE). Thus, the smaller IPCE value is likely to result from the slower electron transfer from I^-/I_3^- to $ZnP^{\bullet+}$ than the electron transfer to $H_2P^{\bullet+}$ because of the smaller driving force of the electron transfer.

On the other hand, we replaced C_{60} with C_{70} as an electron acceptor in the composite electrode system. C_{70} is a rugby ball sphere and may have different steric effects on the accommodation of C_{70} between two porphyrin rings as compared to C_{60}. Figure 7B shows the comparison of IPCE values between OTE/SnO_2/(H_2PC15MPC+C_{60})$_m$ and OTE/SnO_2/(H_2PC15MPC+C_{70})$_m$. The IPCE values of OTE/SnO_2/(H_2PC15MPC+C_{60})$_m$ are much higher than that of OTE/SnO_2/(H_2PC15MPC+C_{70})$_m$. There are two essential factors in efficient photocurrent generation. One is charge separation between porphyrin and fullerene,[15a] and the other is the resulting hole and electron transport in the thin film. Three-dimensional steric control between porphyrin and fullerene using gold nanoparticles contributes to both the efficient formation of charge separation and the hole and electron transport in the thin film. We have previously reported efficient self-exchange electron transfer of porphyrins[36−39] and fullerenes.[40,41] Such fast self-exchange electron transfer of porphyrins and fullerenes in the molecular clusters with interpenetrating network in the thin film results in efficient hopping of hole and electron in each network. The $\pi-\pi$ interaction may play an important role in the formation of the interpenetrating network of a two-dimensional large π-system (porphyrin) and a three-dimensional large π-system (fullerene). It has been reported that there is virtually no difference in the electron-transfer properties between C_{60} and C_{70}.[42−44] However, the spherical shape of C_{60} is superior to the rugby ball shape of C_{70} in uniformity, not only in forming the supramolecular molecular clusters but also in forming the interpenetrating network for efficient electron hopping, resulting in the larger IPCE values.[45]

Photocurrent Generation Mechanism. The photocurrent generation may be initiated by photoinduced charge separation from the porphyrin singlet excited state ($^1H_2P^*/H_2P^{\bullet+}$ = −0.7 V vs NHE)[33b] to C_{60} ($C_{60}/C_{60}^{\bullet-}$ = −0.2 V vs NHE)[33b] in the porphyrin−C_{60} supramolecular complex (Scheme 2) rather than direct electron injection into the conduction band of the SnO_2 (0 V vs NHE)[34b] system, which is energetically more favorable (vide infra). The electron transfer from $^1H_2P^*$ to C_{60} competes well with the energy transfer to the gold nanoparticles.[11] While the reduced C_{60} injects electrons into the SnO_2 nanocrystallites, the oxidized porphyrin ($H_2P/H_2P^{\bullet+}$ = 1.2 V vs NHE)[34b] undergoes the electron-transfer reduction with iodide ion (I_3^-/I^- = 0.5 V vs NHE)[34b] in the electrolyte.

Scheme 2. Illustration of the Photocurrent Generation Mechanism

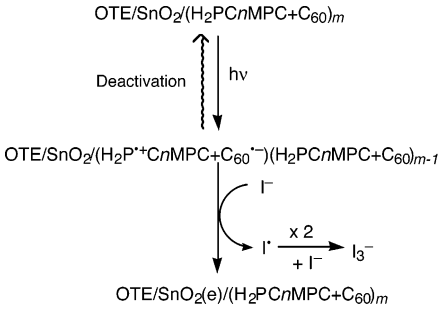

Apparent Association Constants of the Formation of Supramolecular Complexes between H_2PC*n*MPC and C_{60}. The apparent association constants of the formation of supramolecular complexes between H_2PC*n*MPC and C_{60} (eq 2) in mixed solvent (acetonitrile/toluene = 3/1) are determined by the analysis of the fluorescence quenching of H_2PC*n*MPC by C_{60} to estimate the degree of accommodation of C_{60} between two porphyrin rings.[12,18,21,46−49] The results of the fluorescence quenching experiments are shown in Figure 8.

$$(H_2PCnMPC + C_{60})_m \overset{K_{app}}{\rightleftharpoons} (H_2PCnMPC + C_{60})_{m-n'} + n'[H_2PCnMPC + C_{60}] \quad (2)$$

The observed fluorescence quantum yield (ϕ_f(obsd)) of H_2P in cluster solution can be related to the fluorescence yields of uncomplexed (ϕ_f^0) and complexed (ϕ_f') molecules of H_2P by the following equation,[50]

$$\phi_f(\text{obsd}) = (1 - \alpha)\phi_f^{\,0} + \alpha\phi_f' \quad (3)$$

where α is the degree of association between H_2P and C_{60}. Equation 3 can be simplified to the form:

$$\phi_f^{\,0} - \phi_f(\text{obsd}) = \alpha(\phi_f^{\,0} - \phi_f') \quad (4)$$

At relatively high concentrations of C_{60} cluster and [C_{60}] ≫ H_2P, α is given by:

$$\alpha = \frac{K_{app}[C_{60}]}{1 - K_{app}[C_{60}]} \quad (5)$$

From eqs 4 and 5, we obtain the following relation (eq 6).

$$\frac{1}{\phi_f^{\,0} - \phi_f(\text{obsd})} = \frac{1}{\phi_f^{\,0} - \phi_f'} + \frac{1}{K_{app}(\phi_f^{\,0} - \phi_f')[C_{60}]} \quad (6)$$

(36) Fukuzumi, S.; Endo, Y.; Imahori, H. *J. Am. Chem. Soc.* **2002**, *124*, 10974−10975.
(37) Fukuzumi, S.; Hasobe, T.; Endo, Y.; Kei Ohkubo, K.; Imahori, H. *J. Porphyrins Phthalocyanines* **2003**, *7*, 328−336.
(38) Crnogorac, M. M.; Kostic, N. M. *Inorg. Chem.* **2000**, *39*, 5028−5035.
(39) Sun, H.; Smirnov, V. V.; DiMagno, S. G. *Inorg. Chem.* **2003**, *42*, 6032−6040.
(40) Fukuzumi, S.; Nakanishi, I.; Suenobu, T.; Kadish, K. M. *J. Am. Chem. Soc.* **1999**, *121*, 3468−3474.
(41) Thomas, K. G.; Biju, V.; Guldi, D. M.; Kamat, P. V.; George, M. V. *J. Phys. Chem. B* **1999**, *103*, 8864−8869.
(42) Dubois, D.; Kadish, K. M.; Flanagan, S.; Haufler, R. E.; Chibante, L. P. F.; Wilson, L. J. *J. Am. Chem. Soc.* **1991**, *113*, 4364−4366.
(43) Fujitsuka, M.; Luo, C.; Ito, O. *J. Phys. Chem. B* **1999**, *103*, 445−449.
(44) Park, J.; Kim, D.; Suh, Y. D.; Kim, S. K. *J. Phys. Chem.* **1994**, *98*, 12715−12719.
(45) The difference in the electron hopping efficiency between C_{60} and C_{70} clusters appears as a much larger IPCE value of the C_{60} cluster electrode than that of the C_{70} cluster electrode (see Supporting Information S8).

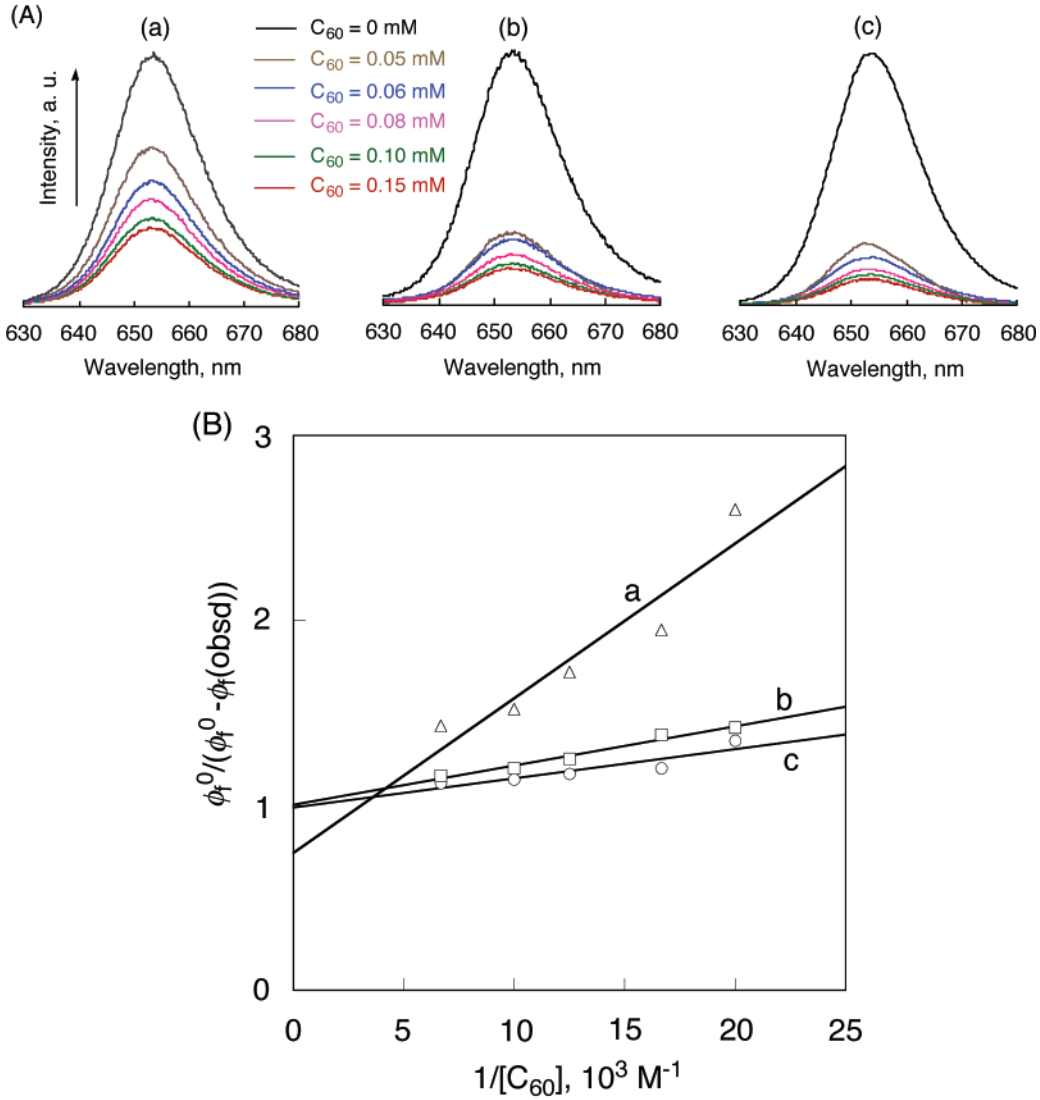

Figure 8. (A) Fluorescence emission spectra of 0.019 mM $H_2PCnMPC$ [(a) $n = 5$, (b) $n = 11$, (c) $n = 15$] in acetonitrile/toluene = 3/1 at various concentrations of C_{60}. The excitation wavelength is 420 nm. (B) Dependence of $\phi_f^0/(\phi_f^0 - \phi_f(obsd))$ on the reciprocal concentration of C_{60} in acetonitrile/toluene = 3/1.

By using eq 6, a linear dependence of $1/(\phi_f^0 - \phi_f(obsd))$ on the concentration of C_{60} clusters is obtained. The K_{app} values of $H_2PC5MPC$, $H_2PC11MPC$, and $H_2PC15MPC$ determined from the double reciprocal plot of Figure 8B are 16 000, 47 000, and 64 000 M^{-1}, respectively. This order of the K_{app} values is consistent with the order of IPCE values of the photocurrent action spectra (vide supra). In addition, the K_{app} value of ZnPC15MPC is determined as 22 000 M^{-1} (see Supporting Information S9), which is much smaller than that of H_2-PC15MPC (64 000 M^{-1}).[51] This indicates that free base porphyrins on gold nanoparticles can easily accommodate C_{60} molecules between two porphyrin rings as compared to zinc porphyrins. The large K_{app} value of $H_2PC15MPC$ relative to ZnPC15MPC leads to the large IPCE values of OTE/SnO_2/(H_2-PC15MPC+C_{60})$_m$ relative to OTE/SnO_2/(ZnPC15MPC+C_{60})$_m$ (Figure 7).

Fluorescence Lifetime Measurements of Thin Films. The fluorescence lifetimes on the OTE/SnO_2 surface were measured by the time-correlated single photon counting technique at emission wavelengths of 650 nm for OTE/SnO_2/(H_2PCn-MPC+C_{60})$_m$ and 605 nm for OTE/SnO_2/(ZnPC*n*MPC+C_{60})$_m$ due to the porphyrin moiety with excitation at 415 nm as shown in Figure S10 (see Supporting Information S10). The decay curve of the fluorescence intensity could be fitted as double exponentials. The fluorescence intensities of OTE/SnO_2/(H_2PCnMPC+C_{60})$_m$ (n = 11, 15) and OTE/SnO_2/(ZnPC15M-PC+C_{60})$_m$ are much lower than those of OTE/SnO_2/(H_2-PC*n*MPC)$_m$ and OTE/SnO_2/(ZnPC15MPC)$_m$, suggesting the occurrence of ultrafast electron transfer from the singlet excited states of porphyrins to C_{60} in the supramolecular complex. Because such a fast process is beyond the time resolution of the present system, the components of fluorescence lifetimes

(46) Kubo, Y.; Sugasaki, A.; Ikeda, M.; Sugiyasu, K.; Sonoda, K.; Ikeda, A.; Takeuchi, M.; Shinkai, S. *Org. Lett.* **2002**, *4*, 925−928.
(47) (a) Jang, W.-D.; Jiang, D.-L.; Aida, T. *J. Am. Chem. Soc.* **2000**, *122*, 3232−3233. (b) Tomioka, N.; Takasu, D.; Takahasahi, T.; Aida, T. *Angew. Chem., Int. Ed.* **1998**, *37*, 1531−1534.
(48) Kimura, M.; Shiba, T.; Yamazaki, M.; Hanabusa, K.; Shirai, H.; Kobayashi, N. *J. Am. Chem. Soc.* **2001**, *123*, 5636−5642.
(49) Kesti, T.; Tkachenko, N. V.; Yamada, H.; Imahori, H.; Fukuzumi, S.; Lemmetyinen, H. *Photochem. Photobiol. Sci.* **2003**, *2*, 251−258.
(50) Kamat, P. V.; Chauvet, J.-P.; Fessenden, R. W. *J. Phys. Chem.* **1986**, *90*, 1389−1394.
(51) The affinity of a free base cofacial porphyrin dimer for C_{60} has also been reported to be larger than that of the corresponding zinc porphyrin dimer; see ref 18b.

in OTE/SnO_2/(H_2PC*n*MPC+C_{60})$_m$ and OTE/SnO_2/(ZnPC15MPC+C_{60})$_m$ may be due to the minor deactivation pathways of the porphyrin excited singlet state. However, the strong fluorescence quenching of OTE/SnO_2/(H_2PC15MPC+C_{60})$_m$ as compared to that of OTE/SnO_2/(H_2PC11MPC+C_{60})$_m$ indicates that more efficient photoinduced electron transfer from the singlet excited state of porphyrins to C_{60} takes place in OTE/SnO_2/(H_2PC15MPC+C_{60})$_m$ than in OTE/SnO_2/(H_2PC11MPC+C_{60})$_m$. This is consistent with the higher IPCE value in OTE/SnO_2/(H_2PC15MPC+C_{60})$_m$. On the other hand, the fluorescence of OTE/SnO_2/(ZnPC15MPC)$_m$ is strongly quenched as compared to the corresponding free base porphyrin system, OTE/SnO_2/(H_2PC15MPC)$_m$ (Figure S10C). This indicates that the singlet excited states of zinc porphyrins are more efficiently quenched by gold nanoparticle or self-quenching or both than that of free base porphyrins. Such strong quenching of the fluorescence of zinc porphyrin on gold nanoparticle results in the lower IPCE value of OTE/SnO_2/(ZnPC15MPC+C_{60})$_m$ (Figure 7A) relative to OTE/SnO_2/(H_2PC15MPC+C_{60})$_m$ (Figure 6B).

Photodynamics of the Composite Molecular Cluster of H_2PC15MPC and C_{60} in Femtosecond Order. The occurrence of ultrafast electron transfer from the singlet excited states of porphyrins to C_{60} in the composite molecular cluster was further confirmed by the femtosecond time-resolved transient absorption spectra of the molecular cluster of H_2PC15MPC and C_{60}. Figure 9A shows time-resolved transient absorption spectra of H_2PC15MPC in toluene. An intense absorption band of the excited singlet state of H_2PC15MPC is observed at 450 nm following the laser pulse excitation. The excited state has a lifetime of 110 ps, as is evident from the decay of the absorption during the first few hundred picoseconds (spectrum a in Figure 9B). Such a decay profile has previously been ascribed to an efficient energy transfer from the porphyrin excited singlet state to the gold nanoparticle.[11] H_2P-ref cluster alone ((H_2P-ref)$_m$) does not exhibit any decay during the time period of 1.5 ns (spectrum b in Figure 9B).

In the case of mixed clusters, however, a new decay pathway that involves quenching of the excited state via electron transfer to C_{60} dominates and further enhances the decay of the porphyrin excited singlet state. The absorption of the singlet excited state of H_2PC15MPC decays within 1.7 ps when the composite cluster of (H_2PC15MPC+C_{60})$_m$ is subjected to laser excitation. The spectral resolution of the (H_2PC15MPC+C_{60})$_m$ composite cluster is complex because of the contributions from porphyrin excited states in H_2PC15MPC and C_{60} excited states and the electron-transfer products in the spectral probe range. Figure 9C shows the time-resolved transient absorption spectra of H_2PC15MPC and C_{60} composite clusters recorded following the laser pulse excitation. The excited singlet state of porphyrin is quenched even at early times, and the absorption spectrum at longer times corresponds to the radical cation of H_2PC15MPC and the radical anion of C_{60} clusters. The small absorption band at 450 nm and the bleaching around the 535 nm region in Figure 9C show the spectral characteristics of transients that are different from those observed for excited singlet state H_2P-ref or H_2PC15MPC. We attribute this absorption band to the radical cation of porphyrin. The absorption spectrum of the stable H_2P-ref radical cation (Figure 9D) was independently measured by oxidizing H_2P-ref with $Fe(bpy)_3^{3+}$ (bpy = 2,2′-bipyridine). The absorption at early times in the 750 nm region arises from the triplet excited state of C_{60} which is formed in small amounts during laser pulse excitation of the composite cluster. However, as the triplet absorption quickly decays, we see a residual absorption arising from the electron-transfer products. For example, the C_{60} radical anion ($C_{60}^{\bullet-}$) has an absorption maximum in the infrared region and is not accessible under the current detection setup. However, $C_{60}^{\bullet-}$ has significant absorption in the red region ((650−750 nm)[40]) and hence can be probed in our laser spectrophotometer.

Figure 9E and F shows the absorption−time profiles recorded at 460 and 700 nm during short and long time duration, respectively. In the case of the (H_2PC15MPC+C_{60})$_m$ composite cluster, we distinctly see a growth of the absorption due to the porphyrin radical cation in H_2PC15MPC with a time constant of 375 fs (spectrum a in Figure 9E). In comparison, the kinetic traces recorded following the laser pulse excitation of individual clusters of H_2P-ref or H_2PC15MPC show a laser pulse limited growth that is significantly faster than the one seen with the composite cluster (spectra c and d in Figure 9E). A transient bleaching is seen in the same probe region (480−550 nm) if we excite C_{60} clusters alone ((C_{60})$_m$) with 387 nm (see Supporting Information S11). Furthermore, the transients recorded at 700 nm show a long-lived transient absorption at longer times for the (H_2PC15MPC+C_{60})$_m$ composite cluster. Both the C_{60} radical anion and the porphyrin radical cation in H_2PC15MPC are expected to contribute to the tail absorption at 750 nm (spectrum a in Figure 9F). It may be noted that the excited-state absorption arising from the excitation of individual species of H_2P on gold nanoparticle and C_{60} (spectra b and c in Figure 9F) at 150 ps is minimal. On the basis of this spectral analysis, we can conclude that the photoinduced electron transfer from the singlet excited state of H_2PC15MPC to C_{60} occurs within 1 ps to produce the porphyrin radical cation in H_2PC15MPC and the C_{60} radical anion in the molecular composite clusters.

Electron Spin Resonance (ESR) Measurements under Photoirradiation. The formation of the radical cation of H_2PC15MPC and the radical anion of C_{60} clusters upon the photoexcitation of the composite cluster of (H_2PC15MPC+C_{60})$_m$ is also confirmed by the electron spin resonance (ESR) measurements performed in frozen acetonitrile/toluene under photoirradiation. The resulting spectrum of photoirradiated (H_2PC15MPC+C_{60})$_m$ in acetonitrile/toluene at 123 K is shown in Figure 10A. The ESR spectrum consists of two signals, one of which is attributable to $C_{60}^{\bullet-}$ at a small g value ($g = 2.002$), and the other is the porphyrin radical cation at a higher g value ($g = 2.003$). To confirm these assignments, the radical cation of H_2P-ref and the radical anion of C_{60} clusters were produced independently via the chemical oxidation of H_2P-ref with $Fe(bpy)_3^{3+}$ and via the photoinduced electron transfer from dimeric 1-benzyl-1,4-dihydronicotinamide to C_{60} clusters,[52] respectively. Their ESR spectra are shown in Figure 10B and C. A comparison of the observed spectrum in Figure 10A with the spectra of the authentic radical cation and radical anion in Figure 10B and C confirms that the observed ESR signal in Figure 10A is composed of two signals, one of which is due to the porphyrin radical cation and the other of which is due to the radical anion of C_{60} clusters.[53]

(52) Fukuzumi, S.; Suenobu, T.; Patz, M.; Hirasaka, T.; Itoh, S.; Fujitsuka, M.; Ito, O. *J. Am. Chem. Soc.* **1998**, *120*, 8060−8068.

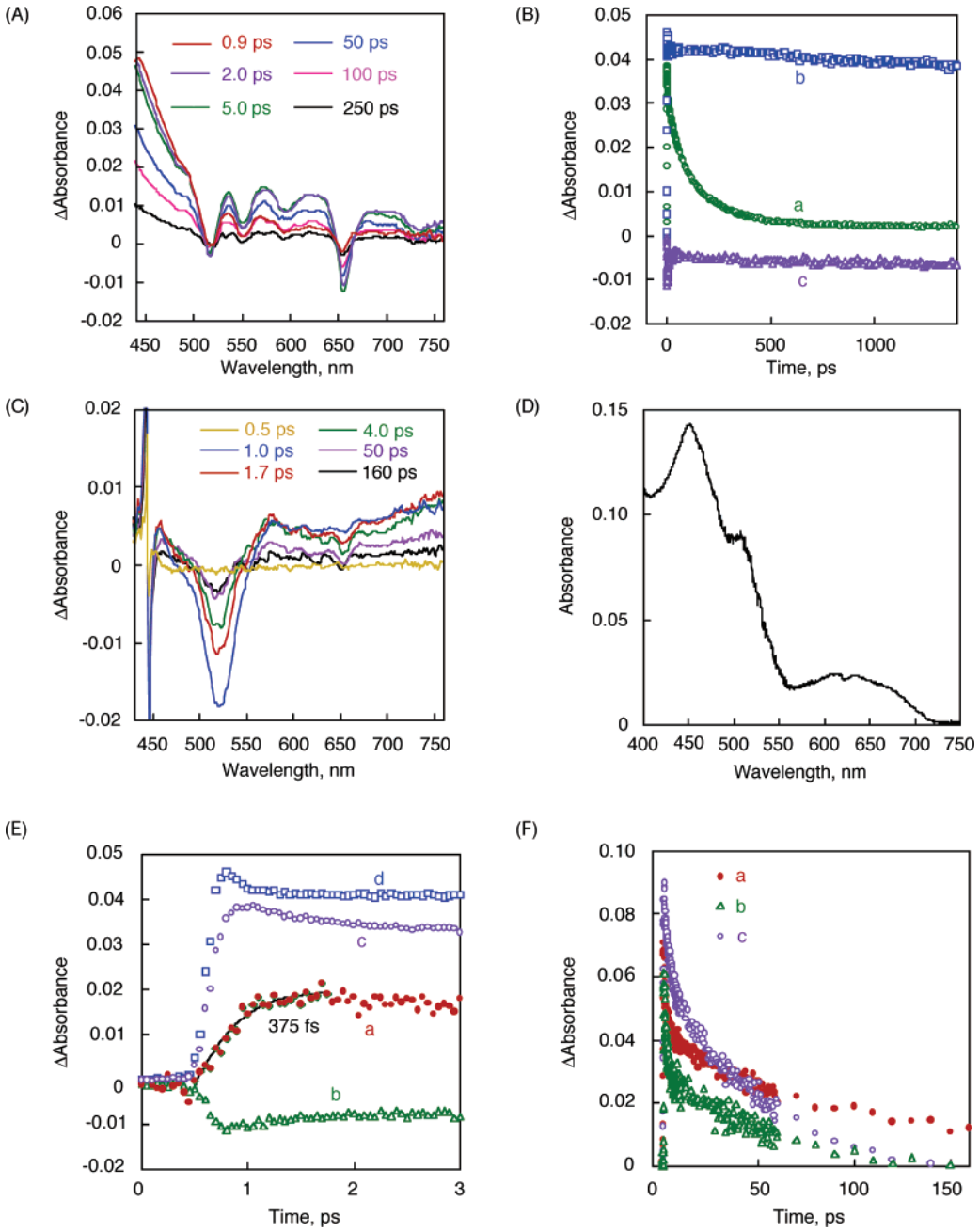

Figure 9. (A) Femtosecond time-resolved absorption spectra of H_2PC15MPC ([H_2P] = 2.0 × 10^{-6} M) in argon-saturated toluene at 298 K after laser excitation at 387 nm. (B) Time profiles of absorption at 460 nm of (a) H_2PC15MPC in toluene ([H_2P] = 2.0 × 10^{-6} M), (b) (H_2P-ref)$_m$ in acetonitrile/toluene = 3/1 ([H_2P] = 0.19 mM), and (c) (C_{60})$_m$ in acetonitrile/toluene = 3/1 ([C_{60}] = 0.31 mM) at 298 K. (C) Femtosecond time-resolved absorption spectra of (H_2PC15MPC+C_{60})$_m$ ([H_2P] = 0.19 mM; [C_{60}] = 0.31 mM) in argon-saturated acetonitrile/toluene (3/1, v/v) after laser excitation at 387 nm at 298 K. (D) Differential spectrum of the radical cation of H_2PC15MPC observed in the electron-transfer oxidation of H_2PC15MPC ([H_2P] = 5.0 × 10^{-6} M) with $Fe(bpy)_3^{3+}$ (1.0 equiv) in deaerated PhCN at 298 K. (E) Absorption decay profiles recorded at 460 nm for (a) (H_2PC15MPC+C_{60})$_m$ (4 times the scale of absorbance for comparison) in argon-saturated acetonitrile/toluene = 3/1 ([H_2P] = 0.19 mM; [C_{60}] = 0.31 mM), (b) (C_{60})$_m$ in argon-saturated acetonitrile/toluene = 3/1 ([C_{60}] = 0.31 mM), (c) H_2PC15MPC in toluene ([H_2P] = 2.0 × 10^{-6} M), and (d) (H_2P-ref)$_m$ in argon-saturated acetonitrile/toluene = 3/1 ([H_2P] = 0.19 mM) at 298 K. (F) Absorption decay profiles recorded at 700 nm for (a) (H_2PC15MPC+C_{60})$_m$ in argon-saturated acetonitrile/toluene = 3/1 ([H_2P] = 0.19 mM; [C_{60}] = 0.31 mM), (b) (C_{60})$_m$ in argon-saturated acetonitrile/toluene = 3/1 ([C_{60}] = 0.31 mM), and (c) H_2PC15MPC in toluene ([H_2P] = 2.0 × 10^{-6} M) at 298 K.

Power Conversion Efficiency of OTE/SnO_2/(H_2PC15MPC+C_{60})$_m$. The photocurrent and photovoltage responses upon the excitation of the OTE/SnO_2/(H_2PC15MPC + C_{60})$_m$ electrode in the visible region (λ > 400 nm) are shown in Figure 11A and B, respectively. The photocurrent response is prompt, steady, and reproducible during repeated on/off cycles of the visible light illumination. The short circuit photocurrent density (I_{sc}) is 1.0 mA/cm^2 and the open circuit voltage (V_{oc}) is 380 mV, and they are reproducibly obtained during the measurements (input power: 11.2 mW/cm^2). Blank experiments conducted with OTE/SnO_2 (i.e., by excluding composite clusters (H_2PC15MPC+C_{60})$_m$) produced no detectable photocurrent under similar experimental conditions.

We have also determined the power conversion efficiency (η) of the photoelectrochemical cell by varying the load resistance (Figure 11C). A drop in the photovoltage and an

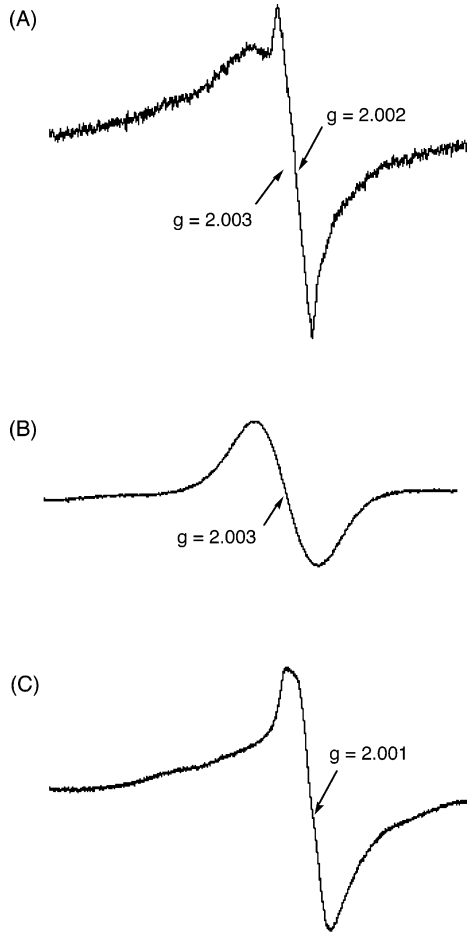

Figure 10. ESR spectra of (A) photoirradiated $(H_2PC15MPC+C_{60})_m$ ($[H_2P]$ = 0.19 mM; $[C_{60}]$ = 0.31 mM) in acetonitrile/toluene (3/1, v/v) with a high-pressure mercury lamp, (B) the radical cation of H_2P-ref (3.0 mM) produced by the electron-transfer oxidation with $Fe(bpy)_3^{3+}$ (3.0 mM) in acetonitrile, and (C) the radical anion of C_{60} clusters $[(C_{60})_m]$ (0.31 mM) generated in photoinduced electron transfer from dimeric 1-benzyl-1,4-dihydronicotinamide (0.31 mM) to C_{60} clusters in acetonitrile/toluene (3/1, v/v) under photoirradiation of a high-pressure mercury lamp, measured at 123 K.

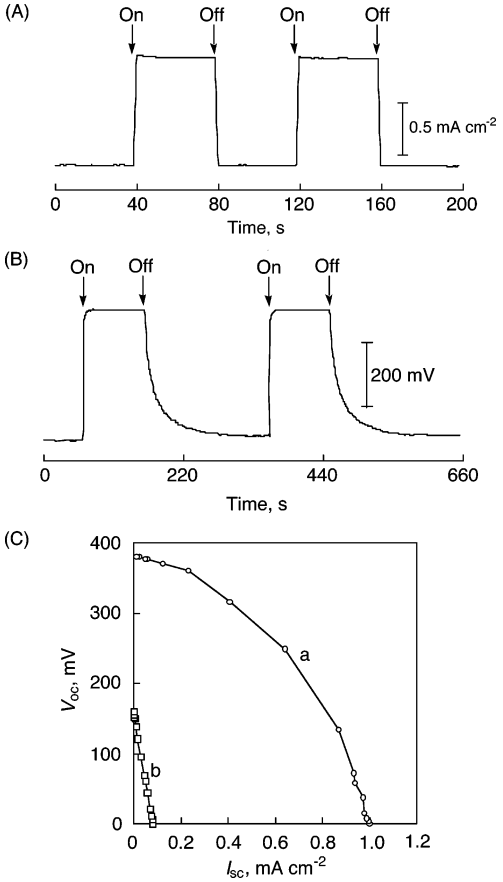

Figure 11. (A) Photocurrent response and (B) photovoltage response of the OTE/SnO_2/$(H_2PC15MPC+C_{60})_m$ electrode prepared from a cluster solution of ($[H_2P]$ = 0.19 mM; $[C_{60}]$ = 0.38 mM) under visible light illumination (λ > 400 nm); electrolyte 0.5 M NaI and 0.01 M I_2 in acetonitrile; input power: 11.2 mW/cm^2. (C) Current−voltage characteristics of (a) the OTE/SnO_2/$(H_2PC15MPC+C_{60})_m$ electrode and (b) the OTE/SnO_2/$(H_2P\text{-ref}+C_{60})_m$ electrode prepared from a cluster solution of ($[H_2P]$ = 0.19 mM; $[C_{60}]$ = 0.38 mM) under visible light illumination (λ > 400 nm); electrolyte 0.5 M NaI and 0.01 M I_2 in acetonitrile; input power: 11.2 mW/cm^2.

increase in the photocurrent are observed with a decrease in the load resistance. The power conversion efficiency, η, is calculated by eq 7,[27]

$$\eta = FF \times I_{sc} \times V_{oc}/W_{in} \qquad (7)$$

where the fill factor (*FF*) is defined as $FF = [IV]_{max}/I_{sc}V_{oc}$, where V_{oc} is the open circuit photovoltage, and I_{sc} is the short circuit photocurrent. The OTE/SnO_2/$(H_2PC15MPC+C_{60})_m$ system has a much larger fill factor (*FF*) of 0.43, open circuit voltage (V_{oc}) of 380 mV, short circuit current density (I_{sc}) of 1.0 mA cm^{-2}, and the overall power conversion efficiency (η) of 1.5% at an input power (W_{in}) of 11.2 mW cm^{-2} as compared to the reference systems (OTE/SnO_2/$(H_2P\text{-ref}+C_{60})_m$). An increase in the alkyl chain length (*n*) of porphyrin-alkanethiol from 11 to 15 in the OTE/SnO_2/$(H_2P15MPC+C_{60})_m$ electrode results in a large improvement of the power conversion efficiency as compared to OTE/SnO_2/$(H_2PC11MPC+C_{60})_m$ (η = 0.61%).[23] The power conversion efficiency (1.5%) of the OTE/SnO_2/$(H_2PC15MPC+C_{60})_m$ system is remarkably enhanced (about 45 times) in comparison with the OTE/SnO_2/$(H_2P\text{-ref}+C_{60})_m$ system (η = 0.035%) under the same experimental conditions.

(53) The slightly larger *g* value (2.002) in Figure 10A as compared to the *g* value of the radical anion of the C_{60} cluster (2.001) may result from the $\pi-\pi$ interaction of $C_{60}^{\bullet-}$ with two porphyrin rings of $H_2PC15MPC$ as shown in Figure 4. Such an interaction lowers the symmetry of $C_{60}^{\bullet-}$, resulting in an increase in the *g* value; see: Fukuzumi, S.; Mori, H.; Suenobu, T.; Imahori, H.; Gao, X.; Kadish, K. M. *J. Phys. Chem. A* **2000**, *104*, 10688−10694.

Conclusion

We have constructed novel organic solar cells by quaternary self-organization of porphyrin and fullerenes with gold nanoparticles. The highly colored composite clusters of porphyrin gold nanoparticles and fullerenes have been assembled as three-dimensional arrays onto nanostructured SnO_2 films using an electrophoretic deposition method. The composite cluster electrode exhibits an incident photon-to-photocurrent efficiency (IPCE) as high as 54% and broad photocurrent action spectra (up to 1000 nm). An increase in the alkyl chain length of porphyrin-alkanethiol from 11 to 15 in the OTE/SnO_2/$(H_2PC15MPC+C_{60})_m$ electrode results in a significant improvement of the power conversion efficiency from 0.61% to 1.5%, which is 45 times higher than that of the reference system. Such a remarkable enhancement in the photoelectrochemical performance as well as a broader photoresponse in the visible and infrared relative to the reference systems demonstrate that the

quaternary organization approach of the porphyrin gold nanoparticles and fullerenes provides a novel perspective for the development of efficient organic solar cells.

Acknowledgment. This work was partially supported by Grant-in-Aids for Scientific Research (No. 16205020 to S.F. and No. 16310073 to H.I.) and for COE Research (Osaka University: Integrated Ecochemistry and Kyoto University Alliance for Chemistry) from the Ministry of Education, Culture, Sports, Science, and Technology, Japan. P.V.K. acknowledges the support from the Office of Basic Energy Science of the U.S. Department of the Energy. This is contribution No. NDRL 4525 from the Notre Dame Radiation Laboratory and from Osaka University. The work at Yonsei University was supported by the National Creative Research Initiative Program of the Ministry of Science and Technology of Korea.

Supporting Information Available: Experimental details of femtosecond laser flash photolysis experiments (S1), detailed procedure of the synthesis and characterization of **2**−**4** (S2, S3), particle size distribution of $(H_2PC11MPC)_m$, $(H_2PC11MC+C_{60})_m$, and $(C_{60})_m$ (S4), TEM image of $(ZnPC15MPC+C_{60})_m$ (S5), absorption spectra of the OTE/SnO_2/$(H_2PCnMPC+C_{60})_m$ electrode [$n = 15$, $n = 11$, and $n = 5$] (S6), AFM images of the OTE/SnO_2/$(H_2PC15MPC+C_{60})_m$ electrode and the OTE/SnO_2/$(H_2PC5MPC+C_{60})_m$ electrode (S7), photocurrent action spectra of the OTE/SnO_2/$(C_{60})_m$ and OTE/SnO_2/$(C_{70})_m$ electrodes (S8), determination of the K_{app} value of the formation of a supramolecular complex between ZnPC15MPC and C_{60} (S9), fluorescence decay curves of the OTE/SnO_2/$(H_2PCnMPC)_m$ electrode ($n = 11$ and 15), the OTE/SnO_2/$(H_2PCnMPC+C_{60})_m$ electrode ($n = 11$ and 15), the OTE/SnO_2/$(ZnPC15MPC)_m$ electrode, and the OTE/SnO_2/$(ZnPC15MPC+C_{60})_m$ electrode (S10), and femtosecond time-resolved absorption spectra of $(C_{60})_m$ (S11). This material is available free of charge via the Internet at http://pubs.acs.org.

JA047768U